$(\gamma, 2N)$ reaction in ^{12}C

J. C. McGeorge, I. J. D. MacGregor, S. N. Dancer,* J. R. M. Annand, I. Anthony,
G. I. Crawford, S. J. Hall, P. D. Harty, J. D. Kellie, G. J. Miller, R. O. Owens, and P. A. Wallace†
Department of Physics and Astronomy, University of Glasgow, Glasgow, G12 8QQ Scotland

D. Branford and A. C. Shotter
Department of Physics, University of Edinburgh, Edinburgh, EH9 3JZ Scotland

B. Schoch,‡ R. Beck, H. Schmieden, and J. M. Vogt§
Institut für Kernphysik, Johannes-Gutenberg Universität, D-55099 Mainz, Germany
(Received 24 October 1994)

The $^{12}C(\gamma, pn)$ and $^{12}C(\gamma, pp)$ reactions have been measured for photon energies between 80 and 157 MeV using a photon tagging spectrometer and plastic scintillator detectors. The overall energy resolution was ~7 MeV, sufficient to determine the initial shells of the emitted nucleons. Corrections were made for solid angle and threshold effects by means of Monte Carlo simulations. For the (γ, pn) reaction both the missing energy and recoil momentum distributions are largely consistent with a two-nucleon absorption process on p-shell and sp nucleon pairs. For the much smaller $^{12}C(\gamma, pp)$ cross section the reaction mechanism is not yet understood but the recoil momentum distributions suggest that final state interactions are not dominant.

PACS number(s): 25.20.Lj, 27.20.+n

I. INTRODUCTION

It has long been known that pn pair emission is the most likely outcome of nuclear photon absorption for energies around 100 MeV. The discovery that the two nucleons share much of the photon energy and are emitted roughly back to back [1] suggests that absorption takes place on a strongly interacting nucleon pair with the rest of the nucleus acting as a spectator. The (γ, pn) reaction is, therefore, a promising tool for the study of $2N$ correlations in nuclei, but before this can be fully exploited it is necessary to develop a more quantitative understanding of the reaction mechanism.

The quasideuteron model developed by Levinger [2] parametrizes the (γ, pn) cross section in terms of the deuteron cross section. Although somewhat phenomenological, this model contains the basic properties of $2N$ absorption and accounts in a general way for the main features of photoreaction data in this energy range. More detailed calculations by Gottfried [3] and Boato and Gianannini [4] have shown that the $(\gamma,2N)$ cross section can be factorized as a product of two terms, $F(P)$ and S_{fi}. The term $F(P)$ is the probability of finding a nucleon pair in the nucleus with small separation and combined momentum $\mathbf{P}$ before the photon is absorbed. In the absence of final state interactions (FSI), the residual nucleus recoils with momentum $-\mathbf{P}$ after absorption. Only the long range properties of the nucleon wave functions, which can be well approximated by the shell model, influence $F(P)$. In contrast S_{fi} depends on the short range correlations between the two nucleons. Boato and Gianannini [4] have shown that $S_{fi}(\gamma, pn)$ and $S_{fi}(\gamma, pp)$ are sensitive to different aspects of the nucleon-nucleon interaction. Ryckebusch *et al.* [5] have questioned the approximations which lead to factorization of the $(\gamma,2N)$ cross section and their recent unfactorized calculations do give an overall reduction in the magnitude of the cross section, although the shape of the opening angle distribution is not significantly altered.

Most of the previous $(\gamma,2N)$ experiments [6] used continuous bremsstrahlung, which necessitated assumptions about the residual nucleus excitation energy in order to determine the photon energy. Experiments using tagged photons at Bonn [7] and Tokyo [8] did not suffer from this problem but had poor neutron energy resolution making it impossible to distinguish the initial shells of the emitted nucleons. These difficulties have prevented a meaningful comparison with theoretical pn opening angle or recoil momentum distributions. Khodyachikh *et al.* [9], who studied the $^{12}C(\gamma, pn)$ reaction with a diffusion chamber in a magnetic field, partially solved the problem of using continuous bremsstrahlung by selecting events where there was no breakup of the residual ^{10}B. This limits the ^{10}B excitation to be less than 5 MeV. However, the recoil momentum in this experiment was determined from the very short ^{10}B tracks in the diffusion chamber giving rather poor resolution, and this ingenious technique is necessarily limited to valence shell

*Present address: Rolls Royce, Derby, UK.
†Present address: Department of Physical Sciences, Glasgow Caledonian University, Glasgow G4 OBA, Scotland.
‡Present address: Physikalisches Institut, Universität Bonn, Bonn, Germany.
§Present address: Saskatchewan Accelerator Laboratory, University of Saskatchewan, Saskatoon SN7 OWO, Canada.

nucleon emission and very low residual excitation energies.

The experimental situation described above prompted the development of large-solid-angle proton [10] and neutron [11] detectors, with ~5 MeV resolution, for (γ, pn) experiments with the Glasgow-Edinburgh-Mainz (GEM) photon tagging spectrometer [12] installed at the 180 MeV Mainz microtron. The overall resolution is sufficient to determine the shells of the emitted nucleons in $(\gamma,2N)$ reactions and the reaction can be studied for all excitation energies in the residual nucleus. The main aim of the present work is to test the basis of the $2N$ absorption model by determining the recoil momentum distributions for $2N$ emission from known shell pairings and comparing with theory.

Data obtained with this experimental setup for ^{16}O, ^{6}Li, and ^{4}He have been presented elsewhere [13–16]. A preliminary experiment on ^{12}C using a prototype neutron time-of-flight (TOF) array has also been reported [17]. The present paper presents a $^{12}C(\gamma, pn)$ data set obtained with a much improved TOF array. It covers a wider photon energy range and has better statistics, allowing more detailed study of the recoil momentum distributions as a function of photon energy and residual excitation energy. In addition, the new TOF array is equipped with a ΔE detector which permitted separation of protons and neutrons in this arm, thereby enabling data for the $^{12}C(\gamma, pp)$ reaction to be presented.

II. EXPERIMENT

The experiment was carried out at the Mainz microtron [18] using the GEM tagged-photon spectrometer [12] together with two plastic scintillator arrays to detect the emitted nucleons. The setup was almost the same as described previously [13], so only a brief outline is given here.

Bremsstrahlung photons were provided by electrons of 183 MeV from the Mainz microtron passing through a 25 μm thick Al radiator at the entrance to the tagged-photon spectrometer. The photons were tagged using two settings of the spectrometer field to cover the photon energy range 80–157 MeV. The photon beam was collimated to a diameter of 33 mm at the target position giving a tagging efficiency (fraction of the tagged photons reaching the target) of ~0.65. The photon flux was monitored during data-taking runs using an ion chamber placed well downstream of the target, and the tagging efficiency was measured with a large scintillating-glass detector in separate runs at reduced beam intensity. The 91 channels of the tagging spectrometer focal plane detector were multiplexed into 6 TDC's but each channel was connected to a pattern unit so that multiple hits in a single TDC could be recognized.

The graphite target was 152.5±0.8 mg/cm^2 thick and placed 3.8 m downstream of the radiator at 30° to the photon beam. To measure background some data were also taken with the target removed and, in order to calibrate the nucleon detectors, some runs were carried out with a 214.4±0.7 mg/cm^2 perdeuterated polythene (CD_2) target.

Protons were detected in a ΔE-ΔE-E telescope array made up of plastic scintillators [10] which covered angles from 50° to 130° and a total solid angle of ~0.9 sr. The front ΔE scintillator was a single flat sheet of dimensions 250×150×1 mm placed parallel to the photon beam 80 mm from the beam axis. Inclusion of this element in the trigger reduced the number of events which did not originate in the target and also provided fast timing signals which were used to start all TDC's. The rear ΔE array was also parallel to the photon beam, 50 cm from the beam axis, with the E elements close behind. Proton emission angles were derived from differences in the arrival times of light at the ends of the elements in these two layers, giving an angular resolution of 3° FWHM in the polar angle and 5° in azimuth. Proton energy was derived from the pulse amplitude in the E elements and the energy resolution was ~4% FWHM at 60 MeV.

The pulse-height threshold on the E blocks of the ΔE-ΔE-E telescope was equivalent to 8 MeV for protons, but, because of energy losses in the target and ΔE scintillators, the effective proton energy threshold varied between 28 MeV at 90° and 32 MeV at extreme angles.

Particles emitted on the opposite side of the target were detected in the angular range 41° to 139° in an array of 24 plastic scintillators described elsewhere [13,11]. These detectors were all placed at 3 m from the target giving a total solid angle of ~0.9 sr, and particle energies were determined by time of flight. The combined effects of the 100 mm detector thickness and the overall timing resolution gave a neutron energy resolution of about ~6 MeV for 70 MeV neutrons. The angular resolution was about 4° FWHM in the polar angle and 1° in azimuth. Protons, deuterons, and neutral particles were distinguished by the signals from a 400×300×2 mm sheet of plastic scintillator (ΔE_{TOF}) placed parallel to the photon beam and 82 mm from the beam axis.

Due to energy losses in the target and along the flight path to the TOF array the 4 MeV pulse-height threshold in TOF corresponds to an effective proton energy threshold of ~26 MeV, slightly dependent on proton angle. For neutrons a pulse-height threshold equivalent to 14 MeV was applied to the TOF signals in the data analysis in order to reduce the proportion of events in which more than one TOF element fired.

The electronic trigger and data readout arrangements were as described previously [13].

III. DATA ANALYSIS

The data from each tagger TDC were analyzed separately so that most events where more than one focal plane channel fired were retained. Events were only discarded if there was a hit in more than one channel served by the same TDC, and the yields were corrected for this by factors (typically 1.20) calculated from the formula derived by Owens [19].

The energy calibration of the photon-tagging spectrometer and the nucleon detectors has been described elsewhere [10–12]. An overall check is provided by form-

ing a deuterium missing energy ($E_\gamma - T_p - T_n$) spectrum of events from the CD_2 target as shown in Fig. 1. The peak due to events from deuterium is at the correct position and its width shows that the missing energy resolution is $\sim$ 7 MeV FWHM.

Data reduction followed the procedure described in Ref. [13]. In the ΔE-ΔE-E telescope protons were selected from two-dimensional plots of amplitude in the E elements versus front ΔE-E time difference and versus ΔE amplitude. On the TOF side particles which did not fire ΔE_{TOF} were classed as neutrons, and protons were selected from those particles which did fire this detector by means of a cut on a two-dimensional plot of pulse height in TOF versus time of flight. Events with more than one TOF detector hit were discarded, but the yields were corrected by a factor (typically 1.10) calculated on the assumption that only one such hit was correlated with the tagged reaction.

The data were split up into one prompt and three random subsets. The prompt set contained events with a double coincidence between the signals in the tagging spectrometer and both nucleon detectors. In the random sets one or both coincidence times were outside the prompt window. All spectra were derived from the prompt data set and corrected for random contributions by subtracting (with suitable weighting factors—see Ref. [13]) the events in the three random data sets. Correction for events ($\sim$10%) which did not originate in the target was obtained by subtracting suitably normalized spectra derived in an identical manner from the data taken with the target removed. Corrections ($\sim$3%) were also made for the dead time of the trigger system during event readout.

To account for bias introduced to the data by thresholds, energy dependent detection efficiency and limited angular acceptance of the nucleon detectors, and to obtain the factors necessary to transform observed yields into cross sections, two Monte Carlo simulations of the experiment were carried out. One ($2N$) was based on the assumption that the photons are absorbed on a nucleon pair during which the recoil nucleus acts as a spectator. The nucleon pair momentum distributions were derived from harmonic oscillator wave functions with the oscillator parameter β chosen ($\beta = 0.359$ fm^{-2}) to give the correct rms radius [20] for ^{12}C. Because the main part of the P distribution for the pair arises from nucleon momenta below the Fermi momentum, the approximation of using harmonic oscillator wave functions only affects the predictions significantly at very high P values. From ^{12}C$(e, e'p)$ and $(p, 2p)$ experiments [21] it is known that p-shell strength dominates up to an excitation of $\sim$13 MeV, while s-shell strength dominates above $\sim$15 MeV. Therefore, for excitation energies up to 10 MeV it was assumed that both emitted nucleons originate in the p shell and that, above 17 MeV one comes from the s shell. In the transition region in between, whose width was chosen to match the experimental energy resolution, $F(P)$ was taken to be a linear combination of $F_{1p1p}(P)$ and $F_{1p1s}(P)$ as in Ref. [13]. Above 30 MeV simulations were done in which one or both nucleons come from the 1s shell. Further details of the Monte Carlo generator for $2N$ absorption are given in the Appendix.

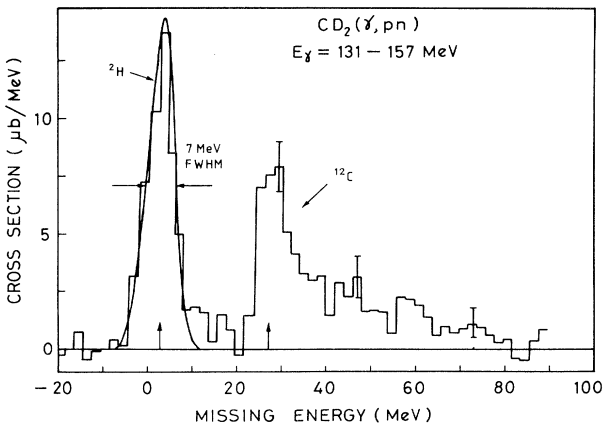

FIG. 1. Deuterium missing energy spectrum observed with a perdeuterated polythene target. The cross section scale applies only to the deuterium peak and is not appropriate for the ^{12}C part of the spectrum. Thresholds for the ^{2}H(γ, pn) and ^{12}C(γ, pn) reactions are indicated by the vertical arrows.

In the other simulation (PH) the available energy was shared amongst the emitted nucleons and the recoil nucleus according to the available phase space.

In the case of a pn pair the proton must be accepted in the proton detector and the neutron in the TOF detector. For a pp pair, as in the actual experiment, either proton may be accepted in the proton detector with the other proton being accepted in the TOF detector. The simulations included calculation of the energy losses suffered by protons before they reach the E element of the telescope or the TOF detector and therefore take account of the angle dependent thresholds discussed above. It was assumed that protons above threshold were always detected but for neutrons an energy dependent detection efficiency was calculated from the STANTON code [22].

For each missing energy bin factors describing the total efficiency of the experiment were obtained from the ratio of detected events to the total number of events generated. These factors were applied to the experimental yields in order to obtain corrected missing energy spectra and to evaluate total cross sections for the reactions.

Uncertainty in the cross sections arises from uncertainties in the neutron detection efficiency ($\sim$10%), and in the target thickness and detector geometry (which together add up to $\sim$4%). Uncertainty in the corrections for dead time and for multiple hits in the tagger and the TOF array were negligible. In the ^{12}C data analysis no corrections were applied for the effects of nuclear interactions of protons with the plastic scintillators. These give rise to a low energy tail in the detector response. In Fig. 1 part of the tail can be seen between the deuterium and carbon peaks. The fraction of events in the tail increases with proton energy [23] and varies between $\sim$1% and $\sim$6% in the present experiments. In missing energy spectra this effect results partly in a reduction of the overall strength and partly in a small shift of strength towards higher missing energy.

As a check the $2N$ Monte Carlo code was modified

slightly in order to simulate the deuterium disintegration events in the CD_2 target and to provide factors to convert the detected yields to angle integrated cross sections. The results (Fig. 2) show good agreement with recent parametrizations of the deuteron cross section [24–26].

In the $2N$ and PH simulations of the recoil momentum distributions required for comparison with the experimental data in Sec. IV, it was necessary to assume a shape for the missing energy distribution. In both cases this was based on the corrected experimental distribution.

IV. RESULTS

A. $^{12}C(\gamma, pn)$ missing energy spectra

Missing energy spectra (E_m) for the $^{12}C(\gamma, pn)$ reaction are shown in Fig. 3, where $E_m = E_\gamma - T_p - T_n - T_r$. Here T_p, T_n, and T_r are the proton, neutron, and recoil kinetic energies and T_r was obtained from the recoil momentum $\mathbf{P}_r = \mathbf{p}_\gamma - \mathbf{p}_p - \mathbf{p}_n$. Corrections for the efficiency of the experimental setup have been applied from both PH and $2N$ simulations. The effect of the uncertainties in the detector thresholds was examined by changing the thresholds in the simulations; the resulting uncertainty in the cross section was found to be $\sim 5\%$ at low E_m and high E_γ and $\sim 20\%$ at the highest E_m. The back-to-back orientation of the nucleon counters is quite efficient for events produced by a $2N$ process and therefore the $2N$ simulation leads to smaller cross sections than the PH simulation. Despite this the shapes of the derived E_m spectra are very similar. The peak near the reaction threshold and the smaller but significant strength extending to higher energies, first noted in our earlier work [17,13] on ^{12}C and ^{16}O, is now seen to be present at all photon energies between 115 and 157 MeV. At lower photon energies the peak is still visible but the spectrum at higher E_m is cut off by the detector thresholds. The width of the peak ($\sim$10 MeV) is not much greater than the instrumental resolution which confirms our preliminary finding [17] that the residual ^{10}B is often in or near its ground state.

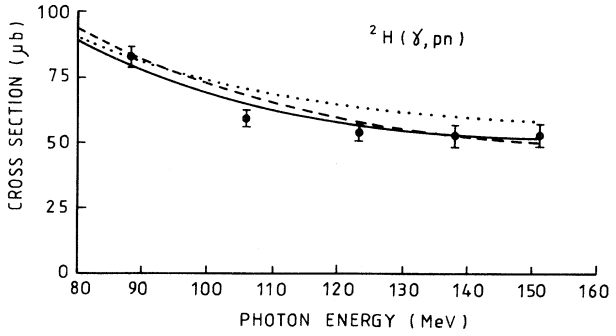

FIG. 2. Total photodisintegration cross section for deuterium. The solid, dashed, and dotted lines represent the parametrizations of previous data from Refs. [24,25,26], respectively.

A first indication of the (γ, pn) reaction mechanism can be obtained from the Dalitz plot of the nucleon and recoil nucleus kinetic energies shown in Fig. 4. For most events the recoil kinetic energy and the difference between proton and neutron kinetic energies are both small, which are the features expected from a $2N$ reaction mechanism. Although the statistics are poorer the Dalitz plot for a higher E_m suggests a broader distribution of $T_1 - T_2$ which could be due to the result of an energy loss by one nucleon during FSI.

If two nucleons are emitted while the rest of the nucleus spectates then the shape of the E_m spectrum can be predicted by folding together two missing energy spectra for single-nucleon knockout. Such spectra are measured in $(e, e'p)$ experiments but the relative strength of the s-shell and p-shell parts varies with the nucleon momentum (P_N) range sampled. A suitable spectrum was constructed from the $(e, e'p)$ data [21] on ^{12}C for

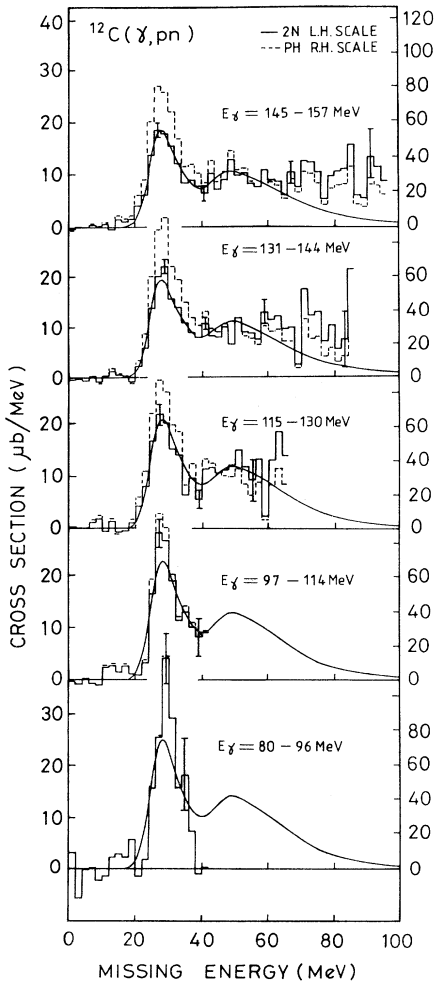

FIG. 3. The $^{12}C(\gamma, pn)$ missing energy spectra corrected for detector geometry and threshold effects using the $2N$ (solid histogram, left scale) and PH simulations (dashed histogram, right scale)—see text. The smooth lines result from folding spectra derived from $^{12}C(e, e'p)$ data as described in the text.

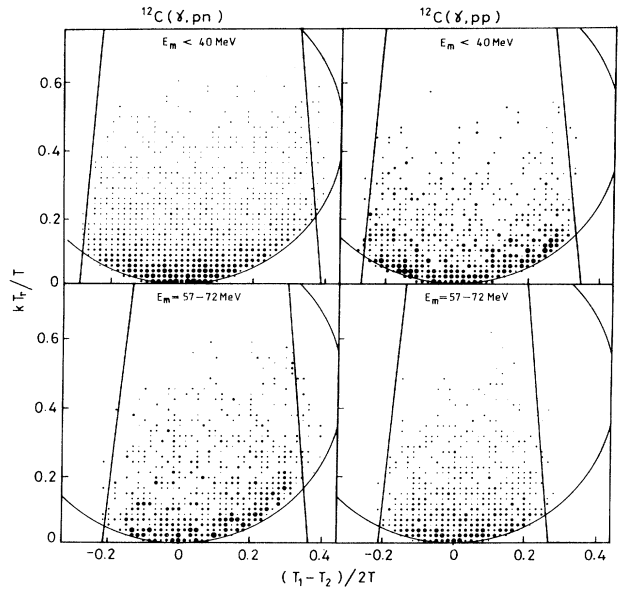

FIG. 4. Dalitz plots for the ^{12}C(γ,pn) and ^{12}C(γ,pp) reactions for $E_\gamma = 133-157$ MeV. The straight lines indicate the detector thresholds. T_1, T_2, T_r, and T are the detected nucleon, recoil and total kinetic energies in the $\gamma+^{12}$C center-of-momentum system and $k = (M_r^2 + M_N M_r)^{\frac{1}{2}}/2M_N T$ where M_N and M_r are the nucleon and recoil rest masses, respectively.

$0 \leq P_N \leq 60$ MeV/c by renormalizing the high energy part of the spectrum so that the relative strengths of the s-shell and p-shell parts were in the ratio of the numbers of s- and p-shell nucleons in ^{12}C. As no ($e,e'n$) data are available, the single-neutron knockout spectrum was approximated by shifting the energy scale of the modified ^{12}C($e,e'p$) spectrum by 4.5 MeV to give the correct ^{12}C(γ,pn) reaction threshold. The result of folding these two spectra together with a 7 MeV FWHM Gaussian to simulate the present experimental resolution is shown by the smooth solid line in Figs. 3 and 5. The dashed line in Fig. 5 results from using the relative pp, sp, and ss absorption strengths at $E_\gamma = 151$ MeV calculated by Ryckebusch *et al.* [5] instead of the numbers of pairs calculated from the shell occupations. The simple calculation gives a good account of the shape of the ^{12}C(γ,pn) missing energy spectra up to ~65 MeV. Although the use of calculated absorption strengths gives a slight improvement at high missing energy, this gives a poorer fit overall. Both predictions underestimate the strength at higher E_m. This may be due to more complex absorption mechanisms or may result from differences between the FSI effects in ($e,e'p$) and (γ,2N) reactions.

It is instructive to compare the cross section integrated over E_m (Table I) with the known [27] total photoabsorption cross section ($\sigma_{\rm tot} \simeq 0.7$ mb at 150 MeV). Because of the truncation of the E_m spectra caused by the nucleon detector thresholds this direct comparison is best done for the highest E_γ bin (145–157 MeV) where the integration can be reliably taken up to $E_m = 90$ MeV. For the 2N mechanism the result (0.690±0.026 mb) confirms that the (γ,pn) channel dominates. The equivalent result from the PH simulation (2.26±0.07 mb) greatly exceeds the total cross section.

Integration of the area under the simulation curve (solid line in Fig. 3) suggests that the (γ,pn) cross section for E_γ=145–157 MeV which is not significantly disturbed by FSI is 0.51±0.02 mb. Comparing with the total absorption cross section [and neglecting contributions other than from (γ,pn)] shows that the combined transmission for both nucleons is about 0.73. Assuming similar proton and neutron transmissions this result is consistent with the lower limit for neutron transmission of 0.81 derived by comparing the (γ,p) and (γ,pn) yields as described by Harty *et al.* [28]. Thus the excess strength at high missing energy can be accounted for, without introducing absorption mechanisms other than

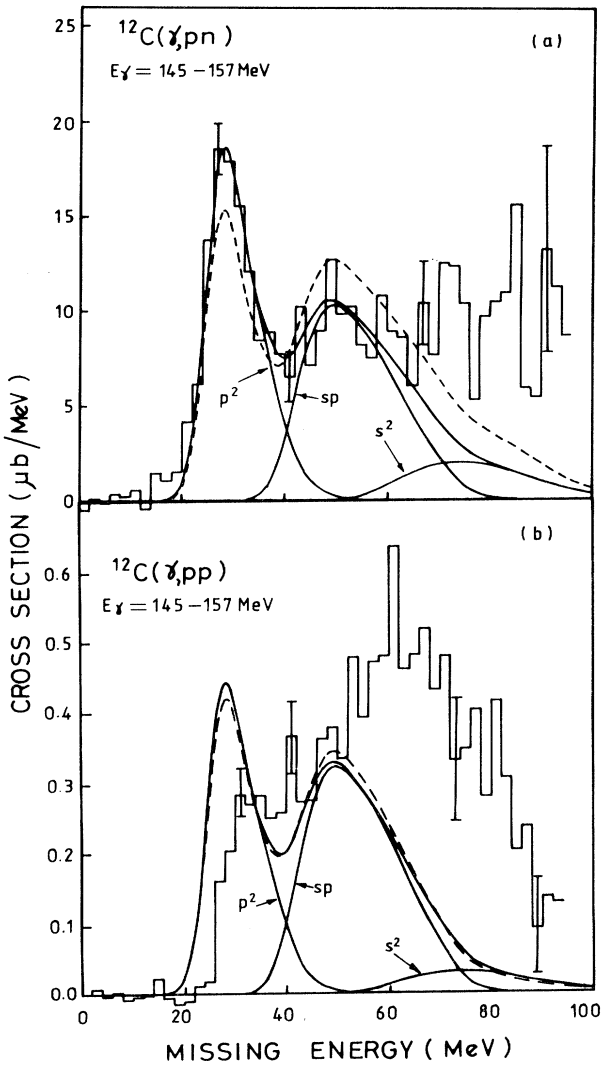

FIG. 5. The ^{12}C(γ,pn) and ^{12}C(γ,pp) missing energy spectra for $E_\gamma = 145-157$ MeV. Correction for detector geometry and threshold effects has been applied using the 2N simulation. The smooth lines result from folding spectra derived from ^{12}C($e,e'p$) data as described in the text.

TABLE I. Cross sections (μb) and ratios (%) for the $^{12}C(\gamma,pp)$ and (γ,pn) reactions assuming a two-nucleon reaction mechanism.

E_γ	80–96 MeV	97–114 MeV	115–130 MeV	131–144 MeV	145–157 MeV
S_{pp}^{40} [a]	-	2.1 ± 0.4	3.9 ± 0.4	3.7 ± 0.3	3.8 ± 0.3
S_{pn}^{40}	322 ± 38	277 ± 16	246 ± 11	237 ± 7	226 ± 7
S_{pp}^{40}/S_{pn}^{40}	-	0.76 ± 0.13	1.58 ± 0.14	1.54 ± 0.12	1.67 ± 0.12
$S_{pp}^{\max}$ [b]	-	-	9.8 ± 0.7	14.1 ± 0.6	22.3 ± 0.7
$S_{pn}^{\max}$	-	-	544 ± 34	625 ± 25	690 ± 26
$S_{pp}^{\max}/S_{pn}^{\max}$	-	-	1.80 ± 0.17	2.26 ± 0.13	3.23 ± 0.16

[a] $S_{px}^{y} = \int_{E_m=0}^{y} \frac{d\sigma(\gamma,px)}{dE_m} dE_m$.

[b] The E_m limits labeled max were 65, 80, and 90 MeV for E_γ=115–130, 131–144, and 145–157 MeV, respectively, chosen to be just below the points at which the spectra were severely cut off by detector thresholds.

$2N$, if events lost at low missing energy due to final state scattering are simply shifted to high missing energy.

B. *pn* pair momentum distributions in ^{12}C

A more quantitative test of the (γ,pn) reaction mechanism can be made by reconstructing the momenta of the recoil nuclei $\mathbf{P}_r = \mathbf{p}_\gamma - \mathbf{p}_p - \mathbf{p}_n$ for the event-by-event data. In the absence of FSI the initial momentum of the pn pair $\mathbf{P}$ is equal to $-\mathbf{P}_r$, and the P distribution can be compared with model predictions derived from the wave functions of the two nucleons. The results [17] of our previous experiments on ^{12}C showed broad consistency with the $2N$ mechanism for photons in the energy range 83–133 MeV. The better statistics and extended photon energy range of the present experiment now allow separate comparisons at different E_γ values and, because higher photon energy data are less affected by detector thresholds, more detailed comparisons at higher missing energy.

Figure 6 shows the $|\mathbf{P}_r|$ distributions for five photon energies for the E_m region below 13 MeV excitation where both nucleons come from the p shell. Also shown are the $2N$ and PH simulations. It is seen that, whereas the PH based calculation fails to account for the shape of the measured distribution, the $2N$ mechanism describes the data well for all the photon energies.

At higher missing energies one or both of the ejected nucleons may come from the s shell. The three different possible shell pairings p^2, sp, and s^2 give rise to different pair momentum distributions. These differences are most evident in the highest E_γ bin (145–157 MeV) where the data are least affected by threshold effects. Figure 7 shows $|\mathbf{P}_r|$ distributions for four regions of E_m. Up to $E_m = 72$ MeV the $2N$ mechanism gives a good account of the data. The different shapes of the $|\mathbf{P}_r|$ distributions are accounted for by the expected initial shell pairings. The PH results clearly fail to account for the distribution for the lowest two E_m cuts, but the differences between the PH and $2N$ distributions become smaller at high E_m. The convergence of the two simulations is due to the combined effects of the reduction in available phase space with increasing missing energy and the effects of detector thresholds which are largest at highest missing energies. The surprisingly good fits to the pair momentum distributions without any corrections for FSI imply that these are small or are such that they completely remove events from the data set (if, for example, the resultant nucleon energy is below threshold).

For the small part of the (γ,pn) cross section at $E_m = 72$–87 MeV the $|\mathbf{P}_r|$ distribution [Fig. 7(d)] does not have the shape characteristic of absorption on an s-shell pair. Although this is the region where absorption on an s-shell pair is expected to be most probable, this result is not surprising in view of the finding (Fig. 5) that only a small part of the high E_m strength can be accounted for as absorption on an s-shell pair. As the PH simulation gives a good account of the data, it may be that most of the events in this region arise from initial absorption on any nucleon pair followed by FSI. However, the $|\mathbf{P}_r|$ data are equally well described by an sp-pair distribution which might suggest that the observed nucleons are emitted from the s and p shells, the high missing energy then being reached by FSI's which do not change $|\mathbf{P}_r|$ significantly. In any case, apart from this small part of the cross section at high E_m, the present $|\mathbf{P}_r|$ data confirm that, for E_γ in the range 80–157 MeV, the major part of the $^{12}C(\gamma,pn)$ cross section arises from absorption on two nucleons.

C. $^{12}C(\gamma,pp)$ missing energy spectra

Missing energy spectra for the $^{12}C(\gamma,pp)$ reaction, obtained with detector acceptance corrections derived from both PH and $2N$ simulations, are shown in Figs. 5(b) and 8. In the $2N$ simulations, it was assumed that the two nucleons both come from the p shell (see Sec. IV D) and that the $2N$ breakup angular distribution in the c.m. frame is the same as for the deuteron. (If one nucleon comes from the s shell and the breakup angular distribution is isotropic the cross sections would be ~20% larger.) As for the (γ,pn) reaction, the (γ,pp) cross section is much larger if a PH simulation is used, but the shape of the missing energy spectrum is again very similar for both PH and $2N$. The strength is seen to increase with increasing missing energy and, in contrast to the (γ,pn) missing energy spectra, there is no peak at low excitation for (γ,pp). The $^{12}C(\gamma,pp)$ cross sections integrated up to

40 MeV (Table I) are significantly smaller than the 10±3 μb found [13] for the p-shell emission region in ^{16}O. The ratio of ^{12}C(γ,pp) to ^{12}C(γ,pn) for the p-shell region is $< 2\%$. However, when the integration over missing energy is taken up to the limits imposed by the detector cutoffs, this ratio is somewhat larger and increases rapidly with E_γ so that the results are not necessarily inconsistent with the larger values (10±2 %) found at higher E_γ by the Tokyo [8] group.

Ryckebusch *et al.* [5] have recently made calculations of ^{12}C(γ,pp) and ^{12}C(γ,pn) cross sections and their ratios over a range of photon energies. The predicted cross sections for both (γ,pp) and (γ,pn) reactions are about a factor of 2 smaller than the present data. The reasons for this are not clear. Nevertheless, it is of interest to compare the calculated ratios with the present experiment because systematic errors in both theoretical and experimental ratios may largely cancel. Figure 9 shows these ratios plotted separately for pp and sp absorption. At low E_m the theory slightly overestimates the ratio whereas at higher E_m it significantly underestimates it. As this calculation contains no (n,p) rescattering mechanism which can transfer initial (γ,pn) strength into the (γ,pp) channel, Fig. 9 suggests that rescattering may be an important contributor to the (γ,pp) reaction, especially at high missing energy.

Attempts to describe the (γ,pp) missing energy spectra by folding the spectra obtained in single nucleon knockout give a poor description of the data [Fig. 5(b)]. As the (γ,pp) cross section is much smaller than the (γ,pn) cross section, it is possible that direct photon absorption on two protons is very weak and that most of the observed (γ,pp) cross section comes from (γ,pn) absorption after which the outgoing neutron suffers a FSI. If this also results in reduction of the emitted nucleon energy it would lead to an apparent increase in strength at high missing energy, as observed. An alternative explanation for the shape of the (γ,pp) missing energy spectrum could be that it results from some mechanism where a third (undetected) particle is also emitted. For example, if quasifree (QF) pion production is followed by a $(\pi,2N)$

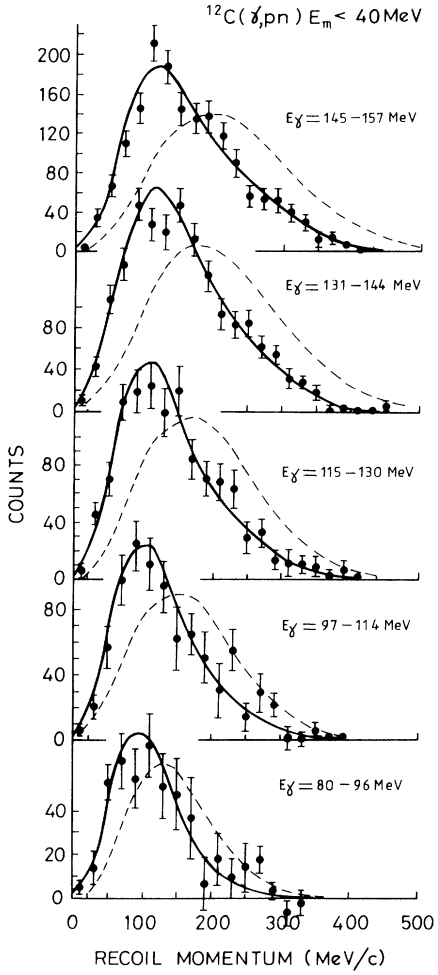

FIG. 6. Observed ^{12}C(γ,pn) recoil momentum distributions for $E_m < 40$ MeV. The solid lines show the results from the $2N$ simulations when absorption takes place on a p-shell nucleon pair. The dashed lines results from the PH simulations.

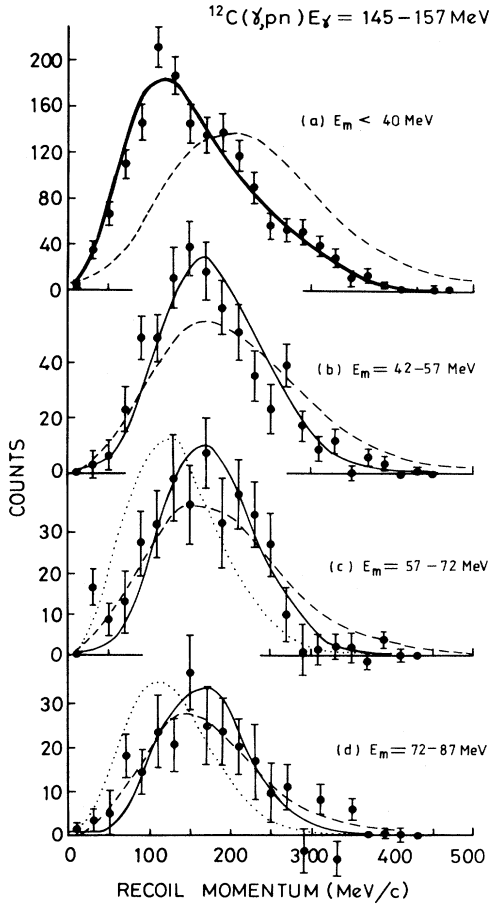

FIG. 7. Observed ^{12}C(γ,pn) recoil momentum distributions for $E_\gamma = 145 - 157$ MeV and different E_m regions. The thick, thin and dotted lines represent the $2N$ simulations with absorption on p-, sp-, and s-shell nucleon pairs, respectively. The dashed lines represent the PH simulations.

reaction, the nucleon emitted in the QF process may go undetected. Such processes can be expected to lead to a smearing of any structure and a shift to higher missing energy, due to the energy carried off by the undetected nucleon, and could therefore explain the different shapes of the (γ, pn) and (γ, pp) missing energy spectra. They can also take place below the pion production threshold if the intermediate pion is virtual.

The Dalitz plot from the (γ, pp) data for low E_m (Fig. 4) shows that the recoil energy is always small. The $T_1 - T_2$ distribution is more spread out compared to the (γ, pn) case and the events are now concentrated away from $T_1 = T_2$ which could be due to reduction of the energy of one nucleon by FSI. As E_m increases the $T_1 - T_2$ distribution becomes more concentrated near zero, and although the detector thresholds restrict the meaningful range of the plot it becomes rather like the low E_m (γ, pn) plot. This surprising result suggests that at high E_m the detected protons come from some kind of $2N$ process and are relatively undisturbed by FSI. This is discussed further in the next section where the observed recoil momentum distributions are presented.

D. *pp* pair momentum distributions in ^{12}C

Recoil momentum distributions for the $^{12}C(\gamma, pp)$ reaction for E_γ=145–157 MeV and for four regions of missing energy are shown in Fig. 10. Also shown are the PH and $2N$ simulations. For $E_m < 40$ MeV the data lie between the $2N$ and PH simulations, but are much closer to the $2N$ prediction. This suggests that most events arise from initial photon absorption on a p-shell pp or pn pair with a subsequent FSI in which little energy or momentum is transferred to the residual nucleus. For this low missing energy region little energy is available for such transfer. If this picture is correct, one would expect that at higher E_m the recoil momentum distribution would lie somewhere between the $2N$ prediction for an sp pair and the PH prediction, becoming closer to the latter as E_m is increased. The data for all higher missing energies, however, contain recoil momenta significantly smaller on average than either the PH simulation or the $2N$ simulation for an sp pair. Surprisingly, a $2N$ simulation in which both nucleons come from the p shell gives a much better description of the data. This again could possibly be explained by a QF process in which most of the missing energy is taken by the initial quasifree nucleon and the remaining energy is transferred to the two observed

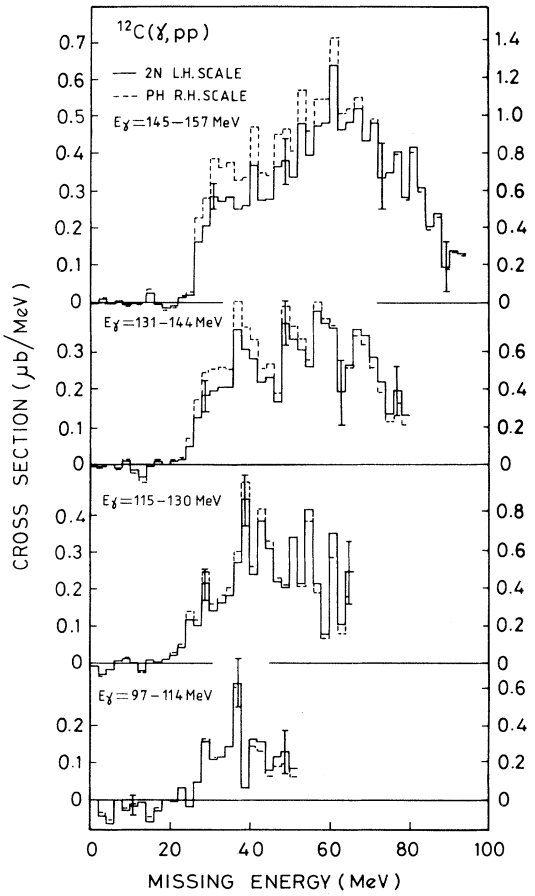

FIG. 8. The $^{12}C(\gamma, pp)$ missing energy spectra corrected for detector geometry and threshold effects using the $2N$ (solid line, left scale) and PH simulations (dashed line, right scale) discussed in the text.

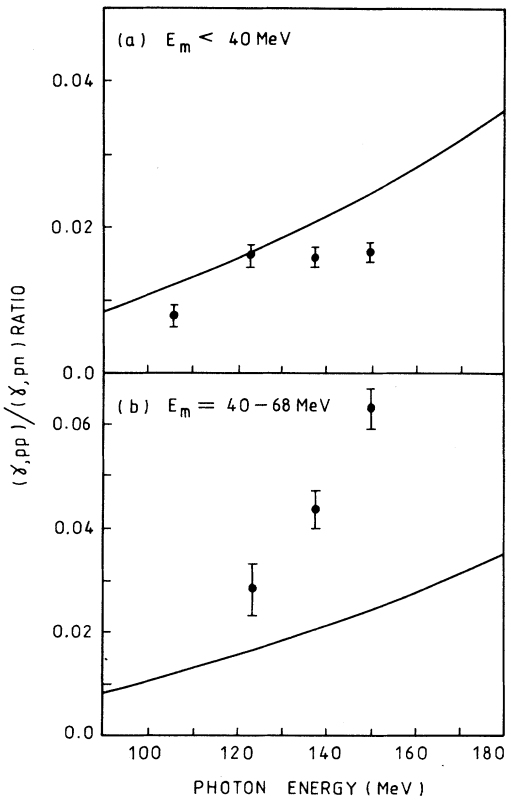

FIG. 9. The $^{12}C(\gamma, pp)/(\gamma, pn)$ cross section ratio as a function of photon energy for missing energy ranges corresponding to (a) p-shell and (b) sp-shell emission. The lines show the results of theoretical calculations by Ryckebusch *et al.* [5].

nucleons by an intermediate pion. If direct photon absorption on two p-shell protons followed by FSI is a major contributor at high E_m then the detected nucleons must lose up to 60 MeV in a way which preserves the initial momentum of the pair.

V. SUMMARY

The 180 MeV GEM tagged-photon spectrometer at the Mainz Microtron has been used with large plastic scintillator detectors to make measurements on the ^{12}C(γ,pn) and (γ,pp) reactions. Missing energy spectra were obtained with resolution sufficient to determine the initial nucleon shells. Recoil momentum distributions for different E_m regions were compared to simulations based on two-nucleon absorption and phase space models. For the (γ,pn) reaction the observed distributions show direct absorption on a p-shell nucleon pair at low E_m and on an sp-pair at higher E_m. Further experiments at higher energy are required to confirm that the 2N mechanism remains appropriate and possibly extract some information about the details of the 2N correlations. Such experiments are already underway [29] with the new 850 MeV Glasgow photon tagging spectrometer [30] installed at the Mainz Microtron MAMI-B [31].

The (γ,pp) cross section increases rapidly with photon energy but is much smaller than the (γ,pn) cross section. The shape of the recoil momentum distribution does not change significantly with missing energy, and is poorly described by a phase space simulation which should be appropriate if final state effects are dominant. A 2N simulation gives a better description of the data if it is assumed that absorption takes place on a pair of p-shell nucleons even at high missing energy where s-shell emission is possible. It is suggested that the (γ,pp) reaction may have important contributions from two step mechanisms [such as quasifree pion production followed by a $(\pi,2N)$ reaction] where the missing energy is lost before the 2N reaction takes place.

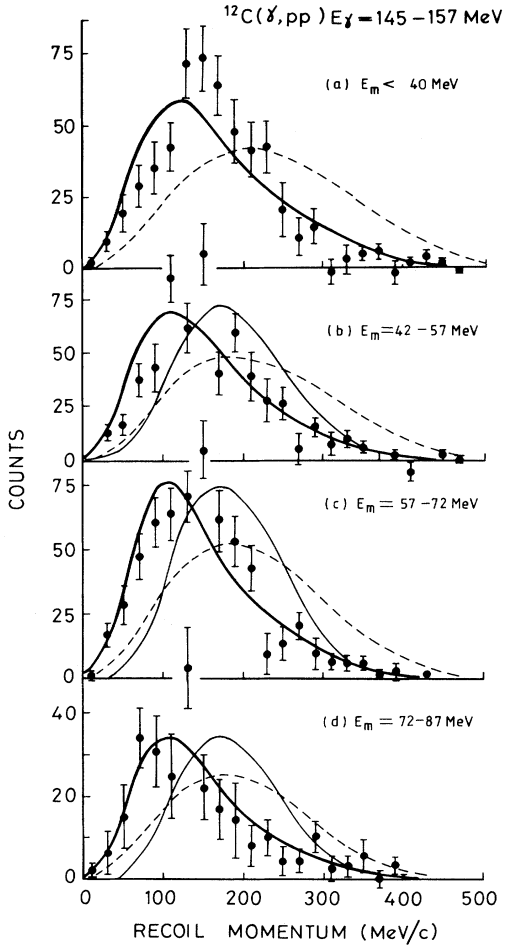

FIG. 10. Observed ^{12}C(γ,pp) recoil momentum distributions for $E_\gamma = 145 - 157$ MeV and different E_m regions. The thick and thin lines represent the 2N simulations with absorption on p-shell and sp-shell pairs, respectively. The dashed lines represent the PH simulations.

ACKNOWLEDGMENTS

This work was supported by the United Kingdom Science and Engineering Research Council and the Deutsche Forschungsgemeinshaft (SFB201). The UK authors wish to thank the Institut für Kernphysik for the use of its facilities and for its assistance during the experiment. Two of us (S.N.D. and P.A.W.) are grateful for financial support from the SERC.

APPENDIX: 2N PHOTON ABSORPTION MODEL

This appendix describes the Monte Carlo 2N photon absorption model which was used to make comparisons with the experimental recoil momentum distributions and to extract cross sections for the (γ,pn) and (γ,pp) reactions. The Monte Carlo event generator described below calculates the momenta of both nucleons ejected from the target following 2N absorption. The events can be sorted into spectra for any desired kinematic variable such as E_m or P, and the spectra can be made with or without the condition that the emitted nucleons are inside the solid angles and have energies above the thresholds of the detectors and are detected.

In the Monte Carlo event generator the photon energy was chosen from a bremsstrahlung distribution weighted by the energy-dependent total photon absorption cross section for deuterium. As the energies involved are well removed from the bremsstrahlung end point energy, the bremsstrahlung distribution was approximated by $1/E_\gamma$. The deuteron cross section was taken from the parametrization of Thorlacius and Fearing [25].

The magnitude of the initial momentum of the interacting nucleon pair was selected from the distribution of $P^2F(P)$, where the nucleon pair momentum distributions for the three possible combinations of initial shells were derived from harmonic oscillator wave functions:

$$F_{1p1p}(P) = \frac{8}{15\sqrt{(2\beta^3\pi)}}\left(3 - \frac{P^2}{\beta} + \frac{P^4}{4\beta^2}\right)\exp\left(-\frac{P^2}{2\beta}\right), \quad \text{(A1)}$$

$$F_{1p1s}(P) = \frac{2}{3\sqrt{(2\beta^3\pi)}}\frac{P^2}{\beta}\exp\left(-\frac{P^2}{2\beta}\right), \quad \text{(A2)}$$

$$F_{1s1s}(P) = \frac{2}{\sqrt{(2\beta^3\pi)}}\exp\left(-\frac{P^2}{2\beta}\right). \quad \text{(A3)}$$

The direction of **P** was chosen from an isotropic distribution. Assuming that the recoil nucleus is a spectator and that there is no FSI, the recoil nucleus has momentum $-\mathbf{P}$ and corresponding kinetic energy T_r.

The excitation of the residual nucleus (E_x) was chosen as described in Sec. III. Maintaining the basic assumption that the residual nucleus is a spectator during the interaction between the photon and the nucleon pair, energy conservation implies that the initial pair has a total energy of $M_t - (M_r + T_r + E_x)$ where M_t and M_r are the rest energies of the target and recoil nuclei, respectively.

After transformation to the center-of-mass frame of the initial nucleon pair and the photon the momenta of the outgoing nucleons were evaluated using energy and momentum conservation. The nucleon directions in this frame were selected assuming either the angular distribution for the $^2\mathrm{H}(\gamma,p)n$ reaction [25] or an isotropic distribution. The nucleon momenta were then transformed back into the laboratory frame. No attempt was made to account for final state effects as the nucleons escape from the nuclear potential well. Because the nucleons are emitted almost back to back the effect on the recoil momentum is expected to be small at the present photon energies.

This $2N$ model has the advantage compared to earlier phenomenological treatments [32,33] of the (γ, NN) process, that overall energy and momentum conservation are guaranteed by a prescription for choosing the energy and momentum of the initial pair, which is also consistent with the spectator role of the residual nucleus.

[1] H. Meyer, A. C. Odian, P. C. Stein, and A. Wattenberg, Phys. Rev. **95**, 576 (1954); M. Q. Barton and J. H. Smith, *ibid.* **95**, 573 (1954).

[2] J. S. Levinger, Phys. Rev. **84**, 43 (1951).

[3] K. Gottfried, Nucl. Phys. **5**, 557 (1958).

[4] L. Boato and M. M. Giannini, J. Phys. G **15**, 1605 (1989).

[5] J. Ryckebusch, M. Vanderhaeghen, L. Machenil, and M. Waroquier, Nucl. Phys. **A568**, 828 (1994).

[6] P. C. Stein, A. C. Odian, A. Wattenberg, and R. Weinstein, Phys. Rev. **119**, 348 (1960), and references therein; I. L. Smith, J. Garvey, J. G. Rutherglen, and G. R. Brooks, Nucl. Phys. **B1**, 483 (1967), and references therein; M. W. Wade, M. K. Brussel, L. J. Koester, and J. H. Smith, Phys. Rev. Lett. **53**, 2540 (1984), and references therein.

[7] J. Arends, P. Detemple, N. Floss, S. Huthmacher, G Kaul, B. Mecking, G. Nöldeke, and R. Stenz, Nucl. Phys. **A526**, 479 (1991); J. Arends, J. Eyink, H. Hartmann, A. Hegerath, B. Mecking, G. Nöldeke, and H. Rost, Z. Phys. A **298**, 103 (1980).

[8] M. Kanazawa, S. Homma, M. Koike, Y. Murata, H. Okuno, F. Soga, N. Yoshikawa, and A. Sasaki, Phys. Rev. C **35**, 1828 (1987), and references therein.

[9] A. F. Khodyachikh, P. I. Vatset, V. N. Gur'ev, I. V. Dogyust, and V. V. Kirichenko, Sov. J. Nucl. Phys. **34**, 789 (1981); I. V. Dogyust, V. I. Voloshchuk, V. V. Kirichenko, and A. F. Khodyachikh, *ibid.* **40**, 878 (1984), and references therein.

[10] I. J. D. MacGregor, S. N. Dancer, J. R. M. Annand, P. A. Wallace, J. D. Kellie, S. J. Hall, and J. C. McGeorge, Nucl. Instrum. Methods A **262**, 347 (1987).

[11] J. R. M. Annand, G. I. Crawford, and R. O. Owens, Nucl. Instrum. Methods. A **262**, 329 (1987).

[12] J. D. Kellie, I. Anthony, S. J. Hall, I. J. D. MacGregor, A. McPherson, P. J. Thorley, S. L. Wan, and F. Zettl, Nucl. Instrum. Methods. A **241**, 153 (1985).

[13] I. J. D. MacGregor *et al.*, Nucl. Phys. **A533**, 269 (1991).

[14] J. M. Vogt, Ph.D. thesis, University of Mainz, 1987; J. M. Vogt *et al.*, in *Proceedings of the 3rd Workshop on Perspectives in Nuclear Physics at Intermediate Energies,* Trieste, edited by S. Boffi, C. Ciofi degli Atti, and M. M. Giannini (World Scientific, Singapore, 1987); S. Klein, Ph.D. thesis, University of Tübingen, 1990.

[15] S. M. Doran *et al.*, Nucl. Phys. **A559**, 347 (1993).

[16] H. Schmieden *et al.*, Phys. Lett. B **314**, 284 (1993).

[17] S. N. Dancer *et al.*, Phys. Rev. Lett. **61**, 1170 (1988).

[18] H. Herminghaus, F. Feder, K. H. Kaiser, W. Manz, and H. v. D. Schmitt, Nucl. Instrum. Methods **138**, 1 (1976); H. Herminghaus, K. H. Kaiser, and U. Ludwig, *ibid.* **187**, 103 (1981).

[19] R. O. Owens, Nucl. Instrum. Methods A **288**, 574 (1990).

[20] H. De Vries, C. W. De Jager, and C. De Vries, At. Data Nucl. Data Tables **36**, 495 (1987).

[21] J. Mougey *et al.*, Nucl. Phys. **A262**, 461 (1976); S. Frullani and J. Mougey, Adv. Nucl. Phys. **14**, 1 (1984).

[22] R. A. Cecil, B. D. Anderson, and R. Madey, Nucl. Instrum. Methods **161**, 439 (1979).

[23] D. F. Measday and C. Richard-Serre, CERN Report CERN 69-17, 1969, p. 1.

[24] P. Rossi *et al.*, Phys. Rev. C **40**, 2412 (1989).

[25] A. E. Thorlacius and H. W. Fearing, Phys. Rev. C **33**, 1830 (1986).

[26] D. A. Jenkins, P. T. Debevec, and P. D. Harty, Phys. Rev. C **50**, 74 (1994).

[27] J. Ahrens, Nucl. Phys. **A446**, 229c (1985); J. Ahrens *et al., ibid.* **A251**, 479 (1975); L. Ghedira, Thése d'Etat de l'Université d'Orsay, Paris X1, 1984; K. P. Schelhaas, J. M. Henneberg, N. Wieloch-Laufenberg, U. Zurmühl, B. Ziegler, M. Schumacher, and F. Wolf, Nucl. Phys. **A506**, 307 (1990).

[28] P. D. Harty, I. J. D. MacGregor, J. C. McGeorge, S. N. Dancer, and R. O. Owens, Phys. Rev. C **47**, 2185 (1993).

[29] P. Grabmayr *et al.*, MAMI-B PAC proposal 1989; I. J. D. MacGregor *et al.*, MAMI-B PAC proposal 1993.

[30] I. Anthony, J. D. Kellie, S. J. Hall, G. J. Miller, and J. Ahrens, Nucl. Instrum. Methods A **301**, 230 (1991).

[31] H. Herminghaus *et al.*, in *Proceedings of the Linear Accelerator Conference*, Albuquerque, 1990 (unpublished).

[32] J. L. Matthews, W. Bertozzi, S. Kowalski, C. P. Sargent, and W. Turchinetz, Nucl. Phys. **A112**, 654 (1968); J. L. Matthews, MIT Laboratory Nuclear Science Internal Report 112, 1967 (unpublished).

[33] H. Schier and B. Schoch, Nucl. Phys. **A229**, 93 (1974).